

See discussions, stats, and author profiles for this publication at: <https://www.researchgate.net/publication/260374284>

Synthesis and structure–activity relationship study of substituted caffeate esters as antinociceptive agents modulating the TREK–1 channel

ARTICLE *in* EUROPEAN JOURNAL OF MEDICINAL CHEMISTRY · JANUARY 2014

Impact Factor: 3.45 · DOI: 10.1016/j.ejmech.2014.01.049 · Source: PubMed

CITATIONS

7

READS

146

11 AUTHORS, INCLUDING:



Vanessa Pereira

French Institute of Health and Medical Rese...

8 PUBLICATIONS 136 CITATIONS

SEE PROFILE



Jerome Busserolles

University of Auvergne

38 PUBLICATIONS 1,071 CITATIONS

SEE PROFILE



Florian Lesage

University of Nice-Sophia Antipolis

117 PUBLICATIONS 10,175 CITATIONS

SEE PROFILE



Alain Eschalier

University of Auvergne

139 PUBLICATIONS 4,672 CITATIONS

SEE PROFILE



Original article

Synthesis and structure–activity relationship study of substituted caffeate esters as antinociceptive agents modulating the TREK-1 channel



Nuno Rodrigues^{a,b}, Khalil Bennis^{b,c}, Delphine Vivier^{a,b}, Vanessa Pereira^{d,e},
 Franck C. Chatelain^f, Eric Chapuy^{d,e}, Hemantkumar Deokar^{b,c}, Jérôme Busserolles^{d,e},
 Florian Lesage^f, Alain Eschalier^{d,e,g}, Sylvie Ducki^{b,c,*}

^a Clermont Université, Université Blaise Pascal, Institut de Chimie de Clermont-Ferrand, BP 10448, F-63000 Clermont-Ferrand, France

^b CNRS, UMR6296, ICCF, F-63171 Aubière, France

^c Clermont Université, ENSCCF, Institut de Chimie de Clermont-Ferrand, BP 10448, F-63000 Clermont-Ferrand, France

^d Clermont Université, Université d'Auvergne, Pharmacologie Fondamentale et Clinique de la Douleur, BP 10448, F-63000 Clermont-Ferrand, France

^e Inserm, UMR1107, Neuro-Dol, F-63001 Clermont-Ferrand, France

^f Labex ICST, Institut de Pharmacologie Moléculaire et Cellulaire, UMR CNRS 7275, Université de Nice Sophia Antipolis, F-06560 Valbonne, France

^g CHU Clermont-Ferrand, Service de pharmacologie, F-63003 Clermont-Ferrand, France

ARTICLE INFO

Article history:

Received 16 October 2013

Received in revised form

13 January 2014

Accepted 19 January 2014

Available online 31 January 2014

Keywords:

TREK-1 channel

Pain

Antinociceptive

Caffeate esters

Structure–activity relationship study

QSAR

Analgesic agents

ABSTRACT

The TWIK-related K⁺ channel, TREK-1, has recently emerged as an attractive therapeutic target for the development of a novel class of analgesic drugs. It has been reported that TREK-1 ^{−/−} mice were more sensitive than wild-type mice to painful stimuli, suggesting that activation of TREK-1 could result in pain inhibition. Here we report the synthesis of a series of substituted caffeate esters (**12a–u**) based on the hit compound CDC **2** (cinnamyl 3,4-dihydroxy- α -cyanocinnamate). These analogs were evaluated for their ability to modulate TREK-1 channel by electrophysiology and for their *in vivo* antinociceptive activity (acetic acid induced-writhing assay) leading to the identification a series of novel molecules able to activate TREK-1 and displaying potent analgesic activity *in vivo*.

© 2014 Elsevier Masson SAS. All rights reserved.

1. Introduction

Ion channels are major drug targets whose study can contribute to the understanding of the physiopathology of pain and the evolution of therapeutic analgesics [1–3]. The TREK-1 (TWIK-related K⁺ channels 1) channel belongs to the two pore-domain potassium (K2P) channel family and was first identified in 1998 [4]. Human TREK-1 is highly expressed in the peripheral sensory system, particularly in small dorsal root ganglion (DRG) neurons that are

associated with nociception [5,6]. The functionality of the TREK-1 channels results from their sensitivity to a variety of stimuli. They are gated by membrane stretching (mechano-activation), pH (intracellular acidosis), temperature (heat), polyunsaturated fatty acids (PUFAs) such as arachidonic acid, and some general volatile anesthetics (chloroform, diethyl ether, and nitrous oxide). They can also be down-modulated by PKA/PKC phosphorylation pathways and tonically inhibited by the actin cytoskeleton [7]. Structurally, the TREK-1 channels are transmembrane (TM) proteins with intracellular N- and C-termini [8]. The pore for K⁺ conduction results from the assembly of two dimers, each containing four helical transmembrane segments (TM1–TM4), arranged in tandem with two pore domains (Fig. 1).

Recent studies have reported that mice with a disrupted TREK-1 gene (TREK-1 ^{−/−}) were more sensitive than wild-type mice to

* Corresponding author. Clermont Université, ENSCCF, Institut de Chimie de Clermont-Ferrand, BP 10448, F-63000 Clermont-Ferrand, France. Tel.: +33 (0) 473407132; fax: +33 (0) 473407008.

E-mail address: Sylvie.Ducki@ensccf.fr (S. Ducki).

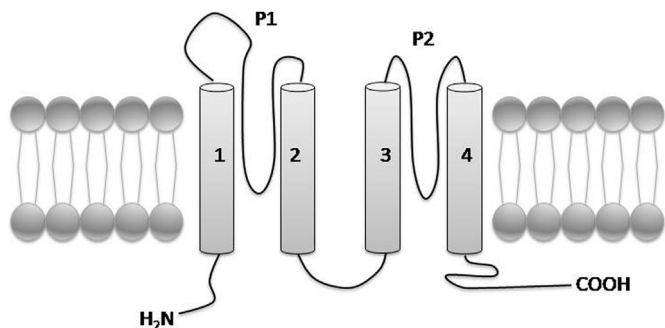


Fig. 1. Topology of TREK-1 channel.

heat and mechanical stimulations [9,10], suggesting that TREK-1 channels are important in pain perception. TREK-1 channel could represent a novel molecular target of interest for the discovery of a new class of analgesics [11].

2. Results and discussion

2.1. Identification of hit molecules

A literature survey allowed us to identify several small organic molecules able to modulate the TREK-1 channels. Riluzole **1** (Fig. 2), a neuroprotective agent currently used in the treatment of amyotrophic lateral sclerosis [12], was reported as an activator of TREK-1 [13,14]. This activation was reported to be transient followed by an inhibition, process attributable to an increase in the intracellular cAMP concentration by riluzole that produces a PKA-dependant inhibition of TREK-1. Cinnamyl 3,4-dihydroxyl- α -cyanocinnamate (CDC **2**, Fig. 2) and caffeic acid phenylethyl ester (CAPE **3**, Fig. 2) were also reported as TREK-1 activators [15]. Danthi et al. carried out a structure–activity relationship (SAR) study but failed to improve the gating activity of the caffeate esters. Because of the reported activities of **2** and **3**, we also decided to consider the CAPE–CDC hybrid molecule **4** [16,17]. Finally, Danthi et al. also reported that polyunsaturated fatty acids, such as linoleic acid **5** (Fig. 2), were able to activate TREK-1 channels [18].

The antinociceptive activity of compounds **1–5** (10 mg/kg, administered subcutaneously) was evaluated by using the acetic acid-induced writhing test in mice. Compared to the controlled mice (vehicle), all the compounds were able to inhibit the induced abdominal writhes (Fig. 3, Table 1). The most active compounds were found to be riluzole **1** (63.6% inhibition) while linoleic acid **5** showed a moderate analgesic activity (29.6% inhibition). CDC **2** showed potent analgesic activity (50.8% inhibition) while CAPE **3** and CDC–CAPE-hybrid **4**, which are structurally similar to **2**, showed low to moderate antinociceptive effect with respectively

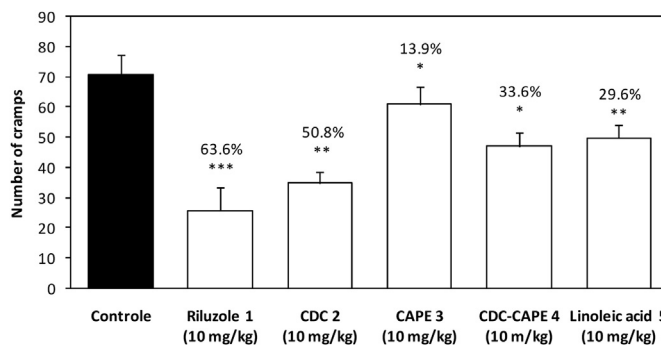


Fig. 3. Antinociceptive effect of compounds **1–5** (10 mg/kg, s.c.) against acetic acid-induced abdominal writhes in mice ($n = 8$). Each bar represents the mean \pm SEM of eight experimental values. The percentage (%) of writhes inhibition (as compared to vehicle) is given above each bar and in Table 1. *t*-Test: * ≤ 0.05 , ** ≤ 0.01 , *** ≤ 0.001 .

13.9% and 33.6% inhibition. This result correlated with the ability of these agents to activate TREK-1, since 10 μ M of CDC is required to increase TREK-1 current by 7-fold compared to 40 μ M of CAPE [15]. These results suggest that the distance between the two aromatic rings and/or the substitution at the α -position of the ester could be an important feature for optimal pharmacological activity.

Although it has been found to possess high analgesic activity, riluzole **1** is non-specific for TREK-1 activation. The drug has been widely studied and many pharmacological activities have been associated with this molecule [19–22]. However no bioactivity data have been reported on CDC **2**, which also displays a good drug-like profile (Fig. 4A and B) [23]. We further evaluated the analgesic activity of CDC **2** in the acetic acid-induced writhing assay and determined an ID_{50} of 8.0 mg/kg (Fig. 4C). No noticeable sedative or adverse effect was observed at the doses tested.

2.2. Synthesis of substituted caffeate esters

Since no information was available about the binding of CDC **2** to the TREK-1 channel, and the 3D structure of TREK-1 was not available at the time, [8] we decided to perform hit optimization by conventional structure–activity relationship (SAR) studies around the general structure **12**, studying the influence of various substituents (R^1 – R^3 , X) on the pharmacological activity of the analogs. We developed two routes to obtain α -substituted cinnamate esters **12** (Scheme 1). Condensation of aldehyde **9** with carbonyl compound **8**, which could be obtained from the carboxylic acid **7** and synthon **6** (route A), would lead to analogs **12** with variations in R^1 , R^2 and X. Alternatively esterification of cinnamic acid derivatives **10** with synthon **6**, the α,β -unsaturated acid emanating from a condensation between aldehyde **9** and carboxylic acid **7** (route B) would lead to analogs **12** bearing different R^3 substituents.

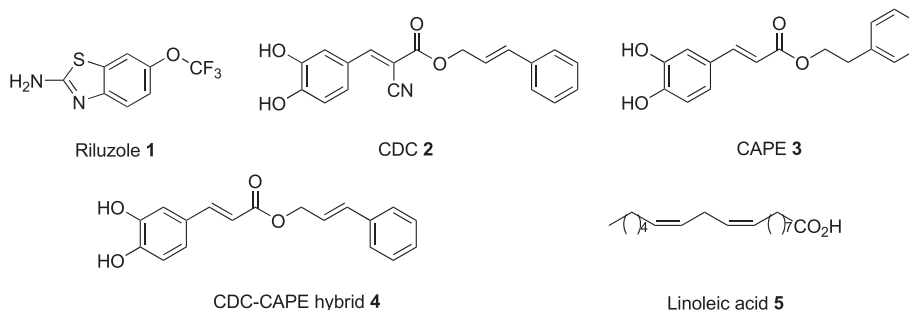


Fig. 2. The chemical structures of compounds **1–5**.

Table 1Antinociceptive activity of compounds **1–5** (10 mg/kg, s.c.) against acetic acid-induced abdominal writhes in mice ($n = 8$).

Compounds	% Writhing inhibition
1	63.6 ± 11.1
2	50.8 ± 5.5
3	13.9 ± 9.4
4	33.6 ± 6.5
5	29.6 ± 8.1

Analogs **12a–p** were prepared through route A (Scheme 2). The appropriately substituted alcohols **6a–k** were reacted with cyanoacetic acid **7a** under coupling conditions (DCC, DMAP, DCM) [17] to yield esters **8a–k** in good to excellent yields (35–98%, Scheme 2A). Alcohol **6a** was subjected to a bromination/alkylation/addition–elimination sequence to give ketone **8l** (41% yield over three steps) and diol **8m** resulted from the opening of epoxide **8e** in 50%

yield under acidic conditions. The corresponding analogs **12a–f** and **12h–q** were obtained by a Knoevenagel condensation under basic conditions between esters **8a–l** and the appropriate benzaldehydes **9a–d** in moderate 30% to excellent 99% yields (Scheme 2B). Acetylation of CDC **2** yielded analog **12g** (80% yield).

Analogs **12r–u** were obtained through route B (Scheme 3). A Wadsworth–Horner olefination [24] between the MOM-protected benzaldehyde **9e** and the appropriately substituted phosphonates **7b,c** afforded, after saponification under basic conditions, the desired MOM-protected caffeic acids **10c–e** in 47 and 74% yield respectively. These acids were coupled to cinnamyl alcohol **6a** and the corresponding esters were deprotected under acidic conditions to give analogs **12r,s** in moderate yields (21 and 46%). Caffeic acid **10e**, obtained in 21% yield from phosphonate **7c** through an olefination/reduction/oxidation sequence, was coupled to **6d** to yield analog **12t** in 64% yield after deprotection. Finally, **10e** was deprotected under acid conditions to afford **12u** in 40% yield.

A

Drugs	Log P	MW	PSA	Log S	Nb rot bonds	HBA	HBD	N atoms
Min [23]	-1	150	20	-4	0	0	0	20
Max [23]	5	500	130	0	9	10	5	70
CDC 2	3.632	321.3	90.6	-3.65	6	5	2	24

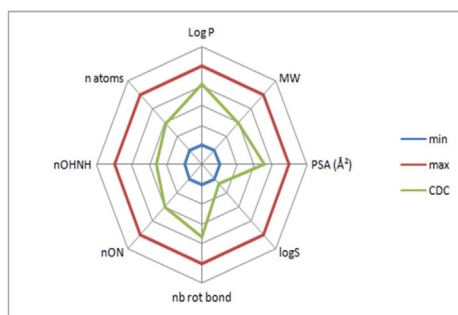
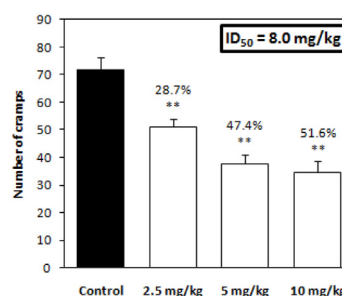
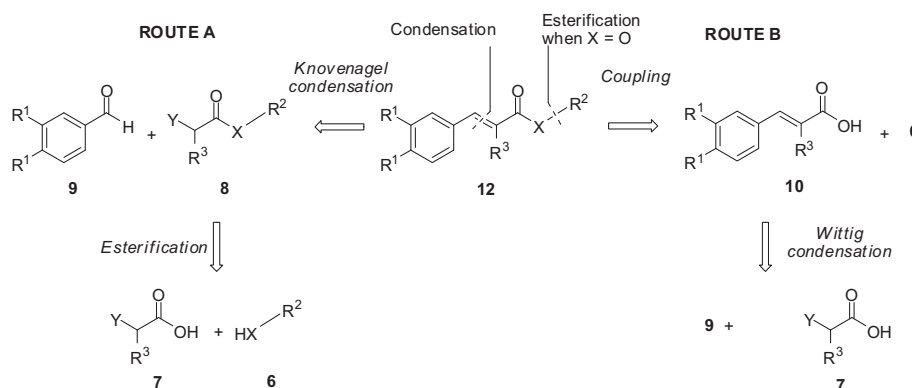
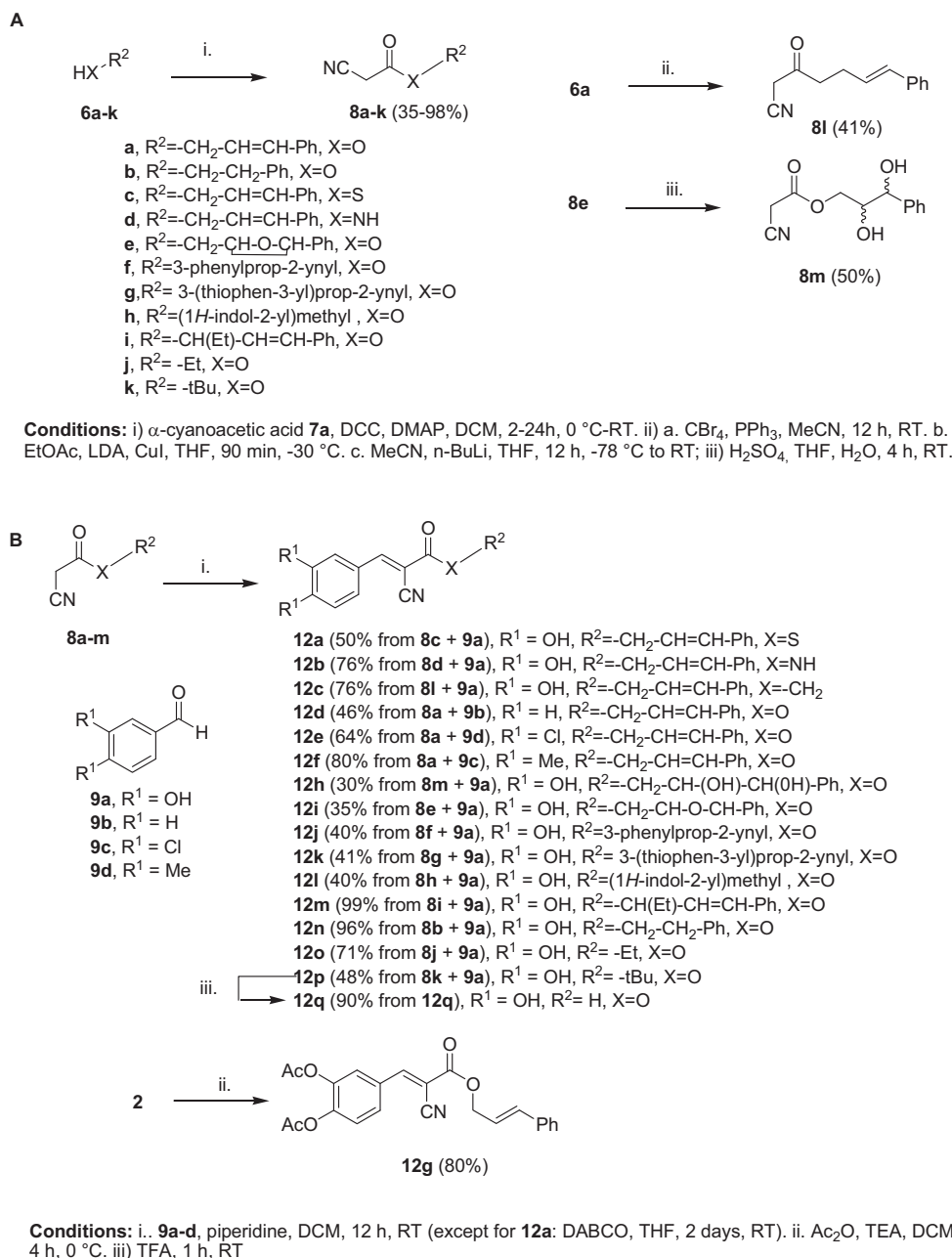
B**C**

Fig. 4. (A) Drug-like properties of CDC **2**. (B) Radar-plot of drug-like properties of CDC **2**. The blue and red lines represent “drug-like” property space [23], and the green line represents the predicted values for CDC **2**. Log P, log of calculated partition coefficient; MW, molecular weight; PSA, polar surface area in Å²; log S, log of predicted solubility score; nb rot bond, number of rotatable bonds; HBA, number of hydrogen-bond acceptors; HBD, number of hydrogen-bond donors; n atoms, number of heavy atoms. (C) Antinociceptive dose response of CDC **2** given subcutaneously against acetic acid-induced abdominal writhes in mice ($n = 8$). Each bar represents the mean ± SEM of eight experimental values. *t*-Test: *≤0.05, **≤0.01, ***≤0.001. (For interpretation of the references to color in this figure legend, the reader is referred to the web version of this article.)

**Scheme 1.** Retrosynthetic analysis of **12**.

Scheme 2. Preparation of **12a–q**.

2.3. Pharmacological evaluation

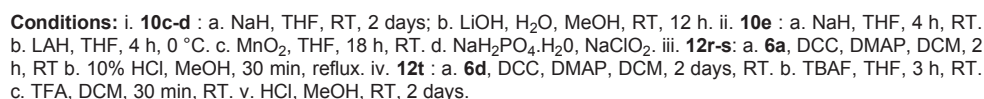
TREK-1 was expressed in *Xenopus* oocytes and the effect of compounds **12a–u** (20 μ M) on channel activity was monitored using the double microelectrode voltage-clamp technique as previously described [25]. Most compounds were able to activate TREK-1 currents at 20 μ M and in all cases, the activation was rapidly reversed following washout of the tested compounds (Table 2). The antinociceptive activity of compounds **12a–u** (10 mg/kg administered subcutaneously) was initially evaluated by using the acetic acid induced-writhing test in mice [26,27]. Apart from two compounds (**12l** and **12r**), the other analogs inhibited the induced abdominal constrictions in the range 5–50%.

The replacement of the ester function of CDC **2** (X = O) by a thioester (**12a**, X = S), an amide (**12b**, X = NH) or a ketone (**12c**,

X = CH₂) resulted in a diminished ability of these compounds to increase TREK-1 current density. We note that this correlated with a decrease in pain inhibition (from 50.8% for **2** to 26.5, 12.3 and 15.0% for **12a–c** respectively).

Next, we varied the substitution R¹ on the aromatic ring (**12d–g**). Substitution of the hydroxyl groups in CDC **2** (R¹ = OH) by hydrogen atoms (**12d**, R¹ = H), electron-donating groups (**12e**, R¹ = CH₃) or electron-withdrawing atoms (**12f**, R¹ = Cl) led to insoluble analogs which could not be evaluated by electrophysiology and their analgesic activity remained moderate (18–31%). CDC **2** (R¹ = OH) was acetylated to give analog **12g** (R¹ = OAc) which resulted in a total loss of TREK-1 activation with retention of a moderate analgesic activity (29%).

Our attention then turned towards the R² side-chain (**12h–q**). Oxidation of the alkene **2** (R² = –CH₂–CH=CH–Ph) into the



Scheme 3. Preparation of **12r–u**.

Analogs **12r–u** varied at the α -position of the carbonyl (R^3). We replaced the α -nitrile varied of the caffeic ester **2** by an α -methyl (**12r**), reduced into the corresponding methylammonium salt **12s** only to find out that these analogs were only moderately able to activate K^+ currents. One compound (**12r**) even worsened the writhes induced by acetic acid while the other (**12s**) retained some ability to reduce the number of writhes induced by acetic acid. Finally among the two compounds (**12t–u**) possessing two structural modifications (R^2 , R^3) compared to the hit compound **2**, the simplified caffeic acid **12u** was able to increase TREK-1 current by almost 3-fold and displayed the most promising anti-nociceptive activity.

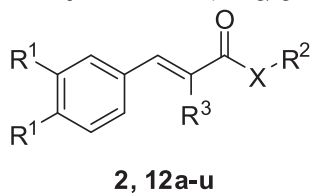
2.4. Pharmacophore identification and atom-based 3D-QSAR

The objective was to develop ligand-based pharmacophore hypotheses (by collecting the common features distributed in a 3D space which represent groups in a molecule that could participate in important interactions with its target) and derive an atom based three-dimensional quantitative structure activity relationship (3D-QSAR) using PHASE (Pharmacophore Alignment and Scoring Engine) [28,29] module from Schrodinger Suite 2010 (to identify atomic features which are responsible for biological activity of novel TREK-1 channel activators).

A total of six pharmacophore hypotheses were generated upon completion of the pharmacophore identification process including AAADD, AAADR, AAARR, AADDR, AADRR, ADDRR. We only selected hypotheses whose scores ranked in the top 1%. Each hypothesis alignment was then used for the atom-based 3D-QSAR model development. The pharmacophore hypothesis with one hydrogen-bond acceptor (A), two hydrogen-bond donors (D) and two aromatic features (R) named ADDRR (Fig. 5) yielded a statistically significant atom-based 3D-QSAR model (Table 4) with an excellent correlation ($R^2 = 0.885$) for the training set (Fig. 6A) and an excellent predictive power ($Q^2 = 0.808$) for test set (Fig. 6B).

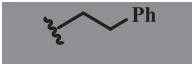



Structural insights into the activity can be gained by visualizing the 3D-QSAR model applied to individual molecules for each chemical characteristic (Fig. 7). In the context of hydrogen-bond donor (D), the 3D-QSAR model clearly indicates that the introduction of alcohols on the ester alkyl chain (*red cubes* (in web version)) is not favorable for activity (Fig. 7A, compounds **2** and **12h**). This is confirmed when these molecules are compared in terms of hydrophobicity (H) (Fig. 7B, molecules **2** and **12h**), suggesting that lipophilicity (*blue cubes* (in web version)) is preferred. The model also suggests that the spatial orientation of the catechol moiety (R^4) in relation to the α,β -unsaturated ester (A1) is a critical feature for high activity (*blue cubes* (in web version)) (Fig. 7B, analogs **2**, **12r**, **12k**). In fact, when the molecules are visualized in the context of their electron withdrawing density (W) (Fig. 7C, compounds **2**, **12c**, **12h**, **12l**), we observed that this feature is important and depends strongly on the spatial orientation of the nitrile ($C\equiv N$)

Table 2
Pharmacological effect of compounds **2**, **12a–u**. a) Modulation of TREK-1 currents expressed in *Xenopus* oocytes as measured by the double microelectrode voltage-clamp technique. R_{TREK-1} is the ratio of the currents measured after and before the application of the compounds **2**, **12a–u** (20 μ M). All the currents were recorded at 0 mV and at the steady state. b) Antinociceptive effect of compounds **2**, **12a–u** (10 mg/kg, s.c.) against acetic acid-induced abdominal writhes in mice ($n = 8$). % Inhibition is the difference between the number of writhes observed in presence and absence of compounds **2**, **12a–u** (10 mg/kg, s.c.).



Compounds	X	R ¹	R ²	R ³	R _{TREK-1}	% Inhibition
2	O	OH		CN	2.64	50.8***
12a	S	OH		CN	1.41	26.5*
12b	NH	OH		CN	1.58	12.3*
12c	CH ₂	OH		CN	1.71	15.0*
12d	O	H		CN	NS ^a	25.1*
12e	O	Me		CN	NS ^a	18.4*
12f	O	Cl		CN	NS ^a	30.7*
12g	O	OAc		CN	0.99	29.0*
12h	O	OH		CN	0.75	24.1**
12i	O	OH		CN	1.47	49.7**
12j	O	OH		CN	2.21	22.0*
12k	O	OH		CN	2.38	5.0*
12l	O	OH		CN	1.00	<0 ^b
12m	O	OH		CN	1.04	45.3*

Table 2 (continued)

Compounds	X	R ¹	R ²	R ³	R _{TREK-1}	% Inhibition
12n	O	OH		CN	1.28	17.0*
12o	O	OH	Et	CN	2.76	21.8*
12p	O	OH	<i>t</i> -Bu	CN	1.17	43.4
12q	O	OH	H	CN	1.23	31.8**
12r	O	OH		CH ₃	1.48	<0 ^b
12s	O	OH		CH ₂ NH ₃ ⁺ Cl [−]	1.27	36.4**
12t	NH	OH		CH ₂ NH ₃ ⁺ TFA [−]	1.05	50.0*
12u	NH	OH	H	CH ₂ NH ₃ ⁺ Cl [−]	2.87	50.1***

t-Test: *≤0.05, **≤0.01, ***≤0.001.

^a NS: not determined because of poor solubility of compound.

^b <0. Compound resulted in increased number of writhes compared to vehicle.

and ester (C=O) functions, suggesting the *S-trans* conformation adopted by the α,β -unsaturated ester is preferred (Fig. 7C, compound **2**, blue cubes (in web version) for C≡N and C=O).

3. Conclusion

We have identified CDC **2** as a lead compound for the development of novel analgesic agents targeting TREK-1 channels. A structure–activity relationship study led us to prepare 21 analogs (**12a–u**), bearing various R¹, R², R³ and X moieties. We developed two synthetic routes to access the desired molecules in 3–12 steps in 3–77% overall yields. Route A provided us with three analogs bearing different X atoms (–O– **2**, –S– **12a**, –NH– **12b**, –CH₂– **12c**), four analogs with various aromatic substitutions R¹ (–OH **2**, –H **12d**, –CH₃ **12e**, –Cl **12f**, –OAc **12g**), and ten analogs bearing R² side-chains (**12a**, **12h–q**), while route B led us to three analogs with various R³ substitution (–CN **2**, –CH₃ **12r**, –CH₂–NH₃⁺ **12s–u**). We note that compounds **12j**, **12k** and **12o** activate TREK-1 channel with R_{TREK-1} > 2 but display little analgesic activity (5–22%), suggesting that they may not be able to reach their target *in vivo*. On

the other hand, compounds **12i** and **12t** display potent analgesic activity (~50%) but are unable to activate the K⁺ channel (R_{TREK-1} < 1.5), suggesting their pharmacological activity is independent or partially dependent on TREK-1 targeting. Finally one analog **12u** proved to be the most potent with high ability to activate TREK-1 channels (R_{TREK-1} = 2.87) and potent analgesic activity (50.1% writhes inhibition) at 10 mg/kg. This α -methyl ammonium substituted caffeic acid could be a potential metabolite of the lead compound **2**. Moreover, this SAR study allowed us to generate a highly predictive atom-based 3D-QSAR model (PHASE) which consists in a five-point pharmacophore hypothesis with one hydrogen-bond acceptor (A), two hydrogen-bond donors (D) and two aromatic features (R). The developed atom-based 3D-QSAR model can provide insights into the structural requirement of novel caffeic acid analogs as activators of TREK-1 channels.

4. Experimental section

4.1. Chemistry

Solvents were distilled prior to use. Other reagents were used as received. Thin layer chromatography analysis (TLC) was performed on pre-coated aluminum backed silica plates Kieselgel 60 F254 (Merck). Spots were visualized under UV light (254 nm) before revealing in an ethanolic solution of phosphomolybdic acid (heating). Purification by column chromatography was carried out on silica gel (70–230 mesh). Melting points were measured by a Reichert plate-heating microscope. ¹H and ¹³C NMR spectra were recorded on a Brücker Avance spectrometer at 400.13 and 100.61 MHz respectively. Chemical shifts δ are reported in ppm relative to solvent residual signal. The coupling constants *J* are given in Hertz (Hz). The abbreviations used for signal descriptions are as follows: s, singlet; d, doublet; t, triplet; q, quartet; m, multiplet. Electron Impact Mass Spectra (EI-MS) were obtained on a spectrometer Hewlett Packard 5989B at 70 eV. High Resolution Electro-spray Ionization Mass Spectra (HR-ESI-MS) were obtained from UBP-Start (Clermont-Ferrand, FRANCE). High performance liquid chromatography (HPLC) conditions for purity analysis [column: Poroshell 120 EC-C18 2.7 μ m (3.0 × 50 mm); temperature column: 40 °C; injection: 10 μ L, 1 mL/min; solvent used H₂O:MeOH mixture with 0.1% TFA (*t* = 0.95% H₂O:5% MeOH, *t* = 1–18 min gradient from 95% H₂O:5% MeOH to 5% H₂O:95% MeOH, 1 min

Table 3

Compounds in training and test sets with observed activity (pR_{TREK-1} obs), number of conformations generated (Nb conf), chemical characteristics (hydrogen-bond acceptor A, hydrogen-bond donor D, hydrophobic/non-polar H, negative ionic N, positive ionic P, aromatic R), and predicted activity for pharmacophore hypothesis ADDRR (pR_{TREK-1} pred).

Compounds	QSAR set	pR _{TREK-1} obs	Nb conf	A	D	H	N	P	R	pR _{TREK-1} pred
2	Training	0.422	61	5	2	1	0	0	2	0.18
12a	Test	0.149	133	5	2	4	0	0	2	0.08
12b	Test	0.199	48	4	3	1	0	0	2	0.19
12c	Training	0.233	122	4	2	1	0	0	2	0.20
12g	Test	−0.004	46	7	0	1	0	0	2	0.02
12h	Training	−0.125	271	7	4	0	0	0	2	0.01
12i	Training	0.167	96	6	2	0	0	0	2	0.11
12j	Test	0.344	47	5	2	1	0	0	2	0.23
12k	Training	0.377	45	5	2	1	0	0	2	0.28
12l	Test	0.000	54	5	3	0	0	0	3	0.04
12m	Training	0.017	60	5	2	2	0	0	2	0.09
12n	Training	0.107	98	5	2	1	0	0	2	0.35
12r	Training	0.167	49	4	2	1	0	0	2	0.35
12s	Training	0.104	79	4	5	1	0	1	2	0.12
12u	Training	0.021	179	4	5	2	0	1	2	0.02

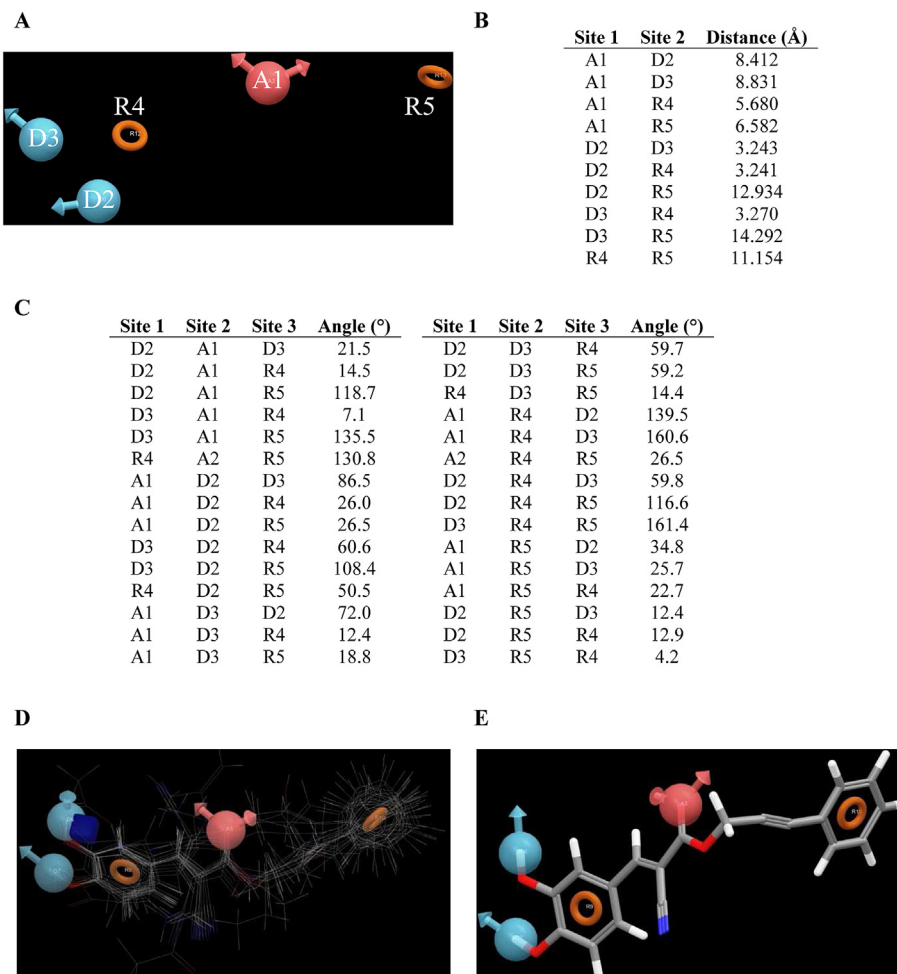


Fig. 5. A. Pharmacophore hypothesis A1D2D3R4R5. B. Distances (in Å) between the pharmacophoric sites of the ADDRR hypothesis. C. Angles (in °) between the pharmacophoric sites of the ADDRR hypothesis. D. All molecules aligned with pharmacophore hypothesis ADDRR. E. The best matched molecule **12j** with pharmacophore hypothesis ADDRR.

isocratic 5% H₂O:95% MeOH), UV detection at 254 nm and 280.5 nm].

4.1.1. (*E*)-Cinnamyl 2-cyano-3-(3,4-dihydroxyphenyl)acrylate **2**

To a solution of cinnamyl 2-cyanoacetate **8a** (82.4 mg, 0.41 mmol, 1.1 eq) in anhydrous DCM under Ar atmosphere was added 3,4-dihydroxybenzaldehyde **9a** (50 mg, 0.373 mmol, 1 eq) and piperidine (cat). The mixture was left to stirred at room temperature until total consumption of cinnamyl 2-cyanoacetate (TLC). The mixture was then quenched by the addition of a saturated aqueous solution NH₄Cl (20 mL) and extracted with EtOAc (3 × 8 mL). The combined organic fractions were dried (Na₂SO₄). After removal of the solvent under reduced pressure, chromatography purification of the residue on silica gel with cyclohexane/EtOAc gave CDC **2** as an orange powder (119.8 mg, 99%). Mp 164 °C.

Table 4

Summary of atom-based 3D-QSAR model for the pharmacophore hypothesis ADDRR which consists of five pharmacophoric sites: one hydrogen-bond acceptor (A), two hydrogen-bond donors (D) and two aromatic features (R).

Training set				Test set		
R ²	SD	F	P	Q ²	RMSE	Pearson-R
0.885	0.058	79.7	4.453e-00.6	0.807	0.0345	0.914

$R_f = 0.50$ (SiO₂, 10% EtOAc/cyclohexane). ¹H NMR (400 MHz, MeOD-*d*₄) δ 8.15 (s, 1H), 7.67 (d, *J* = 2.1 Hz, 1H), 7.44 (d, *J* = 7.3 Hz, 2H), 7.39 (dd, *J* = 2.0, 8.4 Hz, 1H), 7.32 (t, *J* = 7.4 Hz, 2H), 7.25 (t, *J* = 7.3 Hz, 1H), 6.85 (t, *J* = 9.0 Hz, 1H), 6.77 (d, *J* = 15.9 Hz, 1H), 6.41 (dt, *J* = 6.3 and 15.9 Hz, 1H), 4.93 (dd, *J* = 1.0 and 6.4 Hz, 2H). ¹³C NMR (101 MHz, MeOD-*d*₄) δ 164.5, 156.6, 153.2, 147.1, 137.6, 135.8, 129.7, 129.2, 128.2, 127.7, 125.1, 123.7, 117.8, 117.3, 116.7, 98.4, 67.7. HR-ESI-MS calcd for C₁₉H₁₅NO₄ (M + Na⁺) = 344.0899; found 344.0902.

4.1.2. (*E*)-Phenethyl 3-(3,4-dihydroxyphenyl)acrylate **3**

To a solution of (*E*)-4-(3-oxo-3-phenethoxyprop-1-enyl)-1,2-phenylene diacetate **11a** (474 mg, 1.29 mmol, 1 eq) in anhydrous THF (15 mL) was added pyrrolidine (cat). After stirring at room temperature for 30 min, water (10 mL) was added and the reaction mixture was extracted with EtOAc (20 mL). The combined organic layers were washed with 1 N HCl (7 × 20 mL), brine. After drying (Na₂SO₄) and concentration under reduced pressure, CAPE **3** was obtained as a yellow powder (36.7 mg, 75%). Mp 125.5 °C. $R_f = 0.75$ (SiO₂, 40% EtOAc/cyclohexane). ¹H NMR (400 MHz, Acetone-*d*₆) δ 8.36 (br s, 1H), 8.08 (br s, 1H), 7.6 (d, *J* = 15.0 Hz, 1H), 7.40 (dd, *J* = 9.0, 2.0 Hz, 1H), 7.35–7.28 (m, 5H), 7.25 (d, *J* = 2.0 Hz, 1H), 7.20 (d, *J* = 9.0 Hz, 1H), 6.30 (d, *J* = 15.0 Hz, 1H), 4.35 (t, *J* = 7.0 Hz, 2H), 2.90 (t, *J* = 7.0 Hz, 2H). ¹³C NMR (101 MHz, Acetone-*d*₆) δ 167.4, 148.9, 148.4, 145.9, 139.4, 129.9, 129.4, 127.7, 127.3, 122.6, 116.5, 115.6, 115.3, 65.4, 35.9.

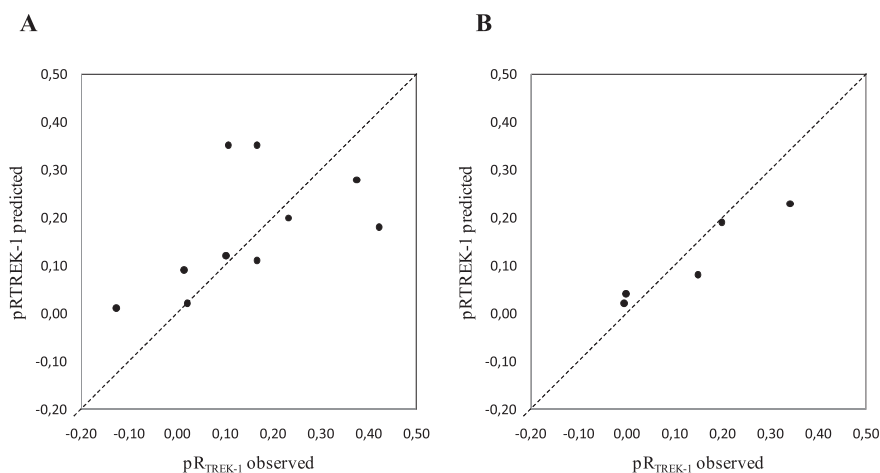


Fig. 6. Graphs of observed versus predicted activity pR_{TREK-1} of (A) training set, (B) test set.

4.1.3. (*E*)-Cinnamyl 3-(3,4-dihydroxyphenyl)acrylate **4**

To a solution of the 4-((*E*)-3-(cinnamyloxy)-3-oxoprop-1-enyl)-1,2-phenylene diacetate **11b** (236.4 mg, 0.622 mmol, 1 eq) in anhydrous THF (7.5 mL) was added pyrrolidine (cat). After stirring at room temperature for 30 min, the reaction was worked up by addition of H_2O (10 mL) and extracted with EtOAc (20 mL). The organic layer was washed with 1 N HCl (7×20 mL), brine. After drying (Na_2SO_4) and concentration under reduced pressure, the

ester was obtained as a yellow powder (181 mg, 98%). Mp 145.5 °C. $R_f = 0.75$ (SiO_2 , 40% EtOAc/cyclohexane). 1H NMR (400 MHz, Acetone- d_6) δ 7.60 (d, $J = 16.0$ Hz, 1H), 7.40 (m, 5H), 7.05 (d, $J = 2.0$ Hz, 1H), 6.96 (dd, $J = 6.0$, 2.0 Hz, 1H), 6.79 (d, $J = 6.0$ Hz, 1H), 6.70 (d, $J = 16.0$ Hz, 1H), 6.40 (dt, $J = 16.0$, 6.0 Hz, 1H), 6.30 (d, $J = 16.0$ Hz, 1H), 4.86 (br s, 2H), 4.82 (d, $J = 6.0$ Hz, 2H). HR-ESI-MS calcd for $C_{18}H_{17}O_4$ ($M + H^+$) = 297.1089; found 297.0932. The NMR data are in agreement with the literature [30].

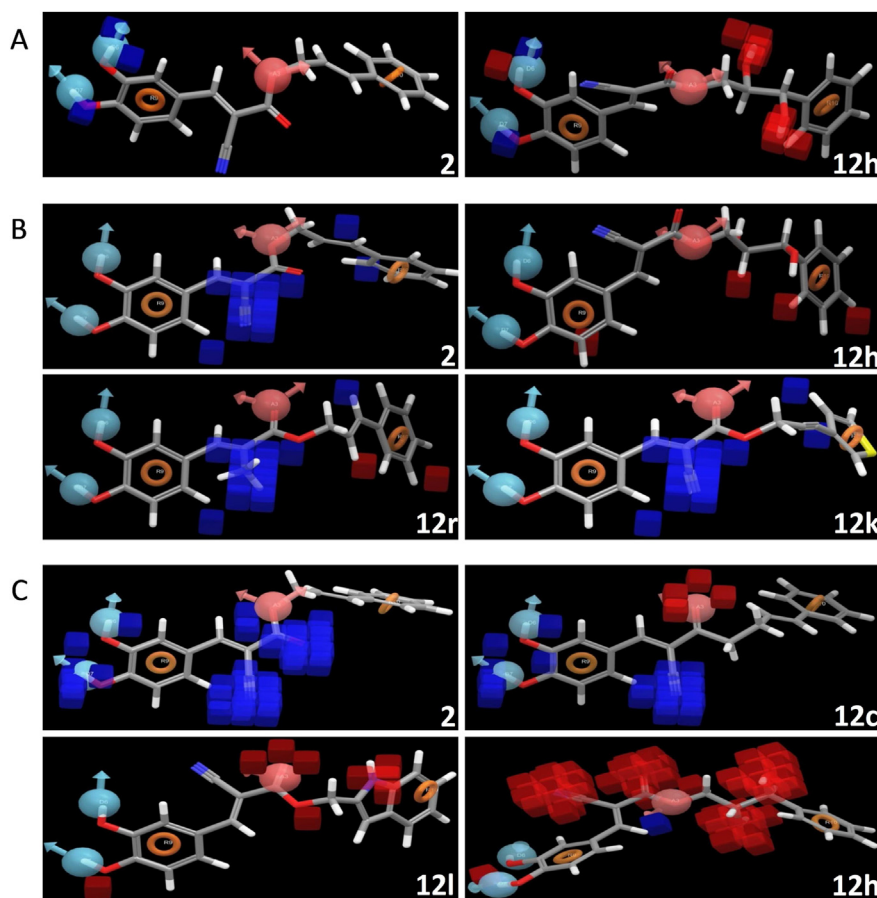


Fig. 7. Pictorial representation of the cubes generated by the QSAR model. Blue cubes indicate favorable regions, while red cubes indicate unfavorable region for the activity. Atom-based 3D-QSAR model visualized in the context of A. Hydrogen-bond donor (D) feature. B. Hydrophobicity (H) and C. Electron-withdrawing density (W). (For interpretation of the references to color in this figure legend, the reader is referred to the web version of this article.)

4.1.4. Cinnamyl 2-cyanoacetate **8a**

To a solution of commercially available cyanoacetic acid **7a** (157.6 mg, 1.85 mmol, 1.1 eq) and cinnamyl alcohol **6a** (192.07 mg, 1.43 mmol, 1 eq) in anhydrous DCM (8 mL) under Ar at 0 °C were added DCC (383 mg, 1.85 mmol, 1.1 eq) and DMAP (cat.). The reaction mixture was stirred for 4 h at 0 °C. The precipitate was filtered and the filtrate was concentrated under reduced pressure. Chromatographic purification of the residue (SiO₂, 50% EtOAc/cyclohexane) gave the ester **8a** as a yellow liquid (296.7 mg, 98%). *R*_f = 0.5 (SiO₂, 30% EtOAc/cyclohexane). ¹H NMR (400 MHz, CDCl₃) δ 7.40–7.30 (m, 5H), 6.68 (d, *J* = 14.8 Hz, 1H), 6.27 (dt, *J* = 15.9, 6.7 Hz, 1H), 4.66 (dd, *J* = 6.8, 1.0 Hz, 2H), 3.49 (s, 2H). ¹³C NMR (101 MHz, CDCl₃) δ 162.9, 135.9, 135.7, 128.7, 128.5, 126.8, 121.4, 113.1, 67.4, 24.8.

4.1.5. (E)-3-(3,4-Diacetoxyphenyl)acrylic acid **10b**

To a cold solution of caffeic acid **10a** (460 mg, 2.55 mmol, 1 eq) and DMAP (7.78 mg, 0.055 mmol, 0.025 eq) in pyridine (1.10 mL) was added acetic anhydride (603 μL, 6.38 mmol, 2.5 eq) under Ar. The mixture was stirred at room temperature for 2 h and poured over crushed ice. The solution was acidified (pH < 2) and extracted with EtOAc (3 × 10 mL). The combined extracts were dried (Na₂SO₄) and concentrated under reduced pressure. Acid **10b** was obtained as a white powder (629.7 mg, 93%). Mp 206 °C. *R*_f = 0.43 (SiO₂, 80% EtOAc/cyclohexane). ¹H NMR (400 MHz, DMSO-*d*₆) δ 12.50 (br s, 1H), 7.30 (m, 3H), 7.31 (d, *J* = 14.0 Hz, 1H), 6.50 (d, *J* = 14.0 Hz, 1H), 2.31 (s, 3H), 2.29 (s, 3H). The NMR data are in agreement with the literature [31].

4.1.6. (E)-4-(3-Oxo-3-phenethoxyprop-1-enyl)-1,2-phenylene diacetate **11a**

To a suspension of diacetylcaffeic acid **10b** (151 mg, 0.572 mmol, 3 eq) in anhydrous toluene (3 mL) were sequentially added 2-phenylethanol **6b** (23.6 μL, 0.197 mmol, 1 eq), DCC (113.8 mg, 0.551 mmol, 2.8 eq) and DMAP (24.1 mg, 0.197 mmol, 1 eq) under Ar. The reaction mixture was heated at 90 °C for 3 h and diluted with EtOAc (10 mL). The mixture was washed with saturated aqueous NaHCO₃ (10 mL) and brine (10 mL). After drying (Na₂SO₄) and concentration under reduced pressure, the residue was purified by flash chromatography (SiO₂, 30% EtOAc/cyclohexane) to afford yellow oil (36.7 mg, 51%). *R*_f = 0.46 (40% EtOAc/cyclohexane). ¹H NMR (400 MHz, CDCl₃): δ 7.60 (d, *J* = 15.0 Hz, 1H), 7.40 (dd, *J* = 10.0, 2.0 Hz, 1H), 7.35–7.25 (m, 5H), 7.25 (d, *J* = 2.0 Hz, 1H), 7.20 (d, *J* = 8.0 Hz, 1H), 6.30 (d, *J* = 15.0 Hz, 1H), 4.35 (t, *J* = 7.0 Hz, 2H), 2.90 (t, *J* = 7.0 Hz, 2H), 2.80 (s, 6H). ¹³C NMR (101 MHz, CDCl₃): δ 168.2, 168.1, 166.6, 143.0, 142.5, 137.9, 133.4, 129.0, 128.6, 126.7, 126.5, 124.0, 122.8, 119.3, 62.3, 35.3, 20.8, 20.7.

4.2. Biological assays

4.2.1. Acetic acid writhing assay

All experiments were performed on 20–24 g male CD1 mice (Janvier, France). All mice were housed in grouped cages in a temperature-controlled environment with food and water *ad libitum*. The behavioral experiments were performed blind to the treatment, in a quiet room, by the same experimenter taking great care to avoid or minimize discomfort of the animals. Animals were randomly divided in groups of 8 mice each and each animal was used only once per compound and euthanized. All animal procedures were approved by the local Animal Ethics Committee and experiments were performed according to the guidelines provided by the European Community guiding in the care and use of animals (86/609/CEE). Animals were pretreated with the compound (10 mg/kg, s.c.) or vehicle (5% Tween 80 in saline (0.9%)) 15 min before injection of acetic acid (0.6% solution, 10 mL/kg) into the

peritoneal cavity of the animal. This activates nociceptors directly and/or produces inflamed viscera (subdiaphragmatic organs) and subcutaneous (muscle wall) of tissues [9]. The number of induced abdominal writhes was determined during 20 min after the injection of acetic acid. The inhibition of abdominal writhes (analgesic effect) is determined by comparing the number of cramps induced in the presence and absence of compound. Additional dose response was performed for compound **2** (CDC) at the following doses: 2.5, 5 and 10 mg/kg (s.c.).

4.2.2. Electrophysiology

Xenopus oocytes deprived of their follicular cells are injected with 50 ng cRNA encoding TREK-1 channel [25]. Eighteen to 24 h after injection, TREK-1 currents are recorded by the technique of the two-microelectrode voltage-clamp technique. In a perfusion chamber of 0.3 mL, the oocyte is impaled with two microelectrodes standards (1–2.5 M resistance) filled with 3 M KCl solution and maintained at a voltage clamp with a Dagan TEV 200 amplifier in a solution standard ND96 (96 mM NaCl, 2 mM KCl, 1.8 mM CaCl₂, 2 mM MgCl₂, 5 mM HEPES, pH 7.4 with NaOH). Then a solution of compound [20 μM, compounds were dissolved in DMSO then diluted in extracellular recording solution (The DMSO concentration in this solution having to be kept below 5%, some compounds were not soluble at concentrations exceeding 10 mM)] is perfused for 15 min, followed by rinsing with ND96 for 6 min. Stimulation of the preparation, data acquisition and analysis were performed using pClamp software.

4.3. Molecular modeling

4.3.1. Pharmacophore modeling

Pharmacophore modeling was carried out using PHASE [28,29] running on Red Hat Linux WS 3.0. A set of 15 novel analogs with determined bioactivity (Table 3) was taken for the development of ligand-based pharmacophore hypothesis and atom-based 3D-QSAR model. The logarithm of the measured *R*_{TREK-1} [*pR*_{TREK-1} = Log (*R*_{TREK-1})] was used in this study. These 15 compounds were divided into a training set (10 compounds) and a test set (5 compounds). The training set molecules were selected in such a way that they contained information in terms of both their structural features and biological activity ranges. In order to assess the predictive power of the model, a set of 5 compounds was arbitrarily set aside as the test set. The test compounds were selected in such a way that they truly represent the training set.

4.3.2. Generation of common pharmacophore hypothesis (CPH)

The common pharmacophore hypothesis (CPH) was carried out by PHASE. All molecules were built in Maestro. All ligands were prepared using LigPrep with the OPLS_2005 force field. Conformational space was explored through combination of Monte-Carlo Multiple Minimum (MCM)/Low Mode (LMOD) with maximum number of conformers 1000 per structure and minimization steps 100. Each minimized conformer was filtered through a relative energy window of 50 kJ/mol and redundancy check of 2 Å in the heavy atom positions. Common pharmacophoric features were then identified from a set of variants (a set of feature types that define a possible pharmacophore) using a tree-based partitioning algorithm with maximum tree depth of four with the requirement that all actives must match. After applying default feature definitions to each ligand (Table 3), common pharmacophores containing three to six sites were generated using a terminal box of 1 Å. Scoring of pharmacophore with respect to activity of ligand was conducted using default parameters for site, vector and volume terms. In atom-based QSAR, a molecule is treated as a set of overlapping van der Waals spheres. Each atom (and hence each sphere) is placed

into one of six categories according to a simple set of rules: hydrogens attached to polar atoms are classified as hydrogen bond donors (D); carbons, halogens, and C–H hydrogens are classified as hydrophobic/non-polar (H); atoms with an explicit negative ionic charge are classified as negative ionic (N); atoms with an explicit positive ionic charge are classified as positive ionic (P); non-ionic atoms are classified as electron-withdrawing (W); and all other types of atoms are classified as miscellaneous (X). For purposes of QSAR development, van der Waals models of the aligned training set molecules were placed in a regular grid of cubes, with each cube allotted zero or more 'bits' to account for the different types of atoms in the training set that occupy the cube. This representation gives rise to binary-valued occupation patterns that can be used as independent variables to create partial least-squares (PLS) QSAR models. Atom-based QSAR models were generated for all hypotheses using the training set using a grid spacing of 1.0 Å. The best QSAR model was validated by predicting activities of the test set molecules.

Author contributions

A.E. and S.D. initiated the project. A.E., J.B., F.L., K.B., S.D. supervised the project, participated in data analysis and manuscript preparation. N.R., D.V. synthesized, purified and characterized the molecules, under the direction of K.B. and S.D. N.R., F.C.C. conducted the electrophysiology experiments under the guidance of F.L. V.P., E.C. conducted behavioral experiments under the guidance of J.B. H.D. conducted the modeling studies under the guidance of S.D.

Acknowledgments

We would like to thank the Regional Council of Auvergne (Conseil Régional d'Auvergne) and the European Fund for Regional Economic Development (FEDER) for a doctoral scholarship for NR; the Novartis Training Scheme for funding a fellowship for DV; the French Ministry of Higher Education and Research (MESR) for a doctoral scholarship for DV; the French National Research Agency (ANR) for funding of the project TREK-ANALGESIA (ANR-12-EMMA-0017-01); LabEx ICST (ANR-11-LABX-0015-01); the Fondation pour la Recherche Médicale (Equipe FRM 2011 to FL); the Société Française d'Etude et de Traitement de la Douleur (SFETD), programme "Groupes de Projets Scientifiques" 2010.

Abbreviations

CAPE	caffeic acid phenethyl ester
CDC	cinnamyl 1–3,4-dihydroxy- α -cyanocinnamate
DABCO	1,4-diazabicyclo[2.2.2]octane
DCC	<i>N,N'</i> -dicyclohexylcarbodiimide
DCM	dichloromethane
DEAD	diethyl azodicarboxylate
DIAD	diisopropyl azodicarboxylate
DMAP	4-dimethylaminopyridine
HBA	hydrogen-bond acceptor
HBD	hydrogen-bond donor
K2P	two-pore domain potassium channel
LAH	lithium aluminum hydride
LDA	lithium diisopropylamide
mCPBA	<i>meta</i> -chloroperoxybenzoic acid
MOM	methoxymethyl
MW	molecular weight
PSA	polar surface area
PTSA	<i>para</i> -toluenesulfonic acid
QSAR	quantitative structure–activity relationship
TBAF	tetrabutylammonium fluoride

TBDMS	<i>tert</i> -butyldimethylsilyl
TEA	triethylamine
TFA	trifluoroacetic acid
TREK	TWIK-related K ⁺ channels
TWIK	tandem of pore domains in a weak inward rectifying K ⁺ channel

Appendix A. Supplementary data

Supplementary data related to this article can be found at <http://dx.doi.org/10.1016/j.ejmech.2014.01.049>.

References

- [1] E. Bourinet, A. Alloui, A. Monteil, C. Barrere, B. Couette, O. Poirot, A. Pages, J. McRory, T. Snutch, A. Eschalier, J. Nargeot, Silencing of the Cav3.2 T-type calcium channel gene in sensory neurons demonstrates its major role in nociception, *EMBO J.* 24 (2005) 315–324.
- [2] T.R. Cummins, P.L. Sheets, S.G. Waxman, The roles of sodium channels in nociception: implications for mechanisms of pain, *Pain* 131 (2007) 243–257.
- [3] D. Julius, A.I. Basbaum, Molecular mechanisms of nociception, *Nature* 413 (2001) 203–210.
- [4] A.J. Patel, E. Honore, F. Maingret, F. Lesage, M. Fink, F. Duprat, M. Lazdunski, A mammalian two pore domain mechano-gated S-type K⁺ channel, *EMBO J.* 17 (1998) 4283–4290.
- [5] F. Maingret, A.J. Patel, F. Lesage, M. Lazdunski, E. Honore, Mechano- or acid stimulation, two interactive modes of activation of the TREK-1 potassium channel, *J. Biol. Chem.* 274 (1999) 26691–26696.
- [6] F. Maingret, E. Honore, M. Lazdunski, A.J. Patel, Molecular basis of the voltage-dependent gating of TREK-1, a mechano-sensitive K⁺ channel, *Biochem. Biophys. Res. Commun.* 292 (2002) 339–346.
- [7] A. Dedman, R. Sharif-Naeini, J.H.A. Folgering, F. Duprat, A. Patel, E. Honore, The mechano-gated K-2P channel TREK-1, *Eur. Biophys. J.* 38 (2009) 293–303.
- [8] W. Treptow, M.L. Klein, The membrane-bound state of K2P potassium channels, *J. Am. Chem. Soc.* 132 (2010) 8145–8151.
- [9] A. Alloui, K. Zimmermann, J. Mamet, F. Duprat, J. Noel, J. Chemin, N. Guy, N. Blondeau, N. Voilley, C. Rubat-Coudert, M. Borsotto, G. Romey, C. Heurteaux, P. Reeh, A. Eschalier, M. Lazdunski, TREK-1, a K⁺ channel involved in polymodal pain perception, *EMBO J.* 25 (2006) 2368–2376.
- [10] J. Noel, K. Zimmermann, J. Busserolles, E. Deval, A. Alloui, S. Diochot, N. Guy, M. Borsotto, P. Reeh, A. Eschalier, M. Lazdunski, The mechano-activated K⁺ channels TRAAK and TREK-1 control both warm and cold perception, *EMBO J.* 28 (2009) 1308–1318.
- [11] (a) J. Noël, G. Sandoz, F. Lesage, Molecular regulations governing TREK and TRAAK functions, *Channels* 5 (2011) 402–409; (b) S.N. Bagriantsev, K.H. Ang, A. Gallardo-Godoy, K.A. Clark, M.R. Arkin, A.D. Renslo, D.L. Minor Jr., A high-throughput functional screen identifies small molecule regulators of temperature- and mechano-sensitive K2P channels, *ACS Chem Biol.* 16 (2013) 1841–1851.
- [12] A. Doble, The pharmacology and mechanism of action of riluzole, *Neurology* 47 (1996) S233–S241.
- [13] F. Duprat, F. Lesage, A.J. Patel, M. Fink, G. Romey, M. Lazdunski, The neuroprotective agent riluzole activates the two P domain K⁺ channels TREK-1 and TRAAK, *Mol. Pharmacol.* 57 (2000) 906–912.
- [14] A. Cadaveira-Mosquera, S.J. Ribeiro, A. Reboreda, M. Perez, J.A. Lamas, Activation of TREK currents by the neuroprotective agent riluzole in mouse sympathetic neurons, *J. Neurosci.* 31 (2011) 1375–1385.
- [15] S. Danthi, J.A. Enyeart, J.J. Enyeart, Caffeic acid esters activate TREK-1 potassium channels and inhibit depolarization-dependent secretion, *Mol. Pharmacol.* 65 (2004) 599–610.
- [16] H. Cho, M. Ueda, M. Tamaoka, M. Hamaguchi, K. Aisaka, Y. Kiso, T. Inoue, R. Ogino, T. Tatsuoka, Novel caffeic acid derivatives: extremely potent inhibitors of 12-lipoxygenase, *J. Med. Chem.* 34 (1991) 1503–1505.
- [17] L.H. Hu, H.B. Zou, J.X. Gong, H.B. Li, L.X. Yang, W. Cheng, C.X. Zhou, H. Bai, F. Gueritte, Y. Zhao, Synthesis and biological evaluation of a natural ester sinterin and its synthetic analogues, *J. Nat. Prod.* 68 (2005) 342–348.
- [18] S. Danthi, J.A. Enyeart, J.J. Enyeart, Modulation of native TREK-1 and Kv1.4 K⁺ channels by polyunsaturated fatty acids and lysophospholipids, *J. Membr. Biol.* 195 (2003) 147–164.
- [19] C.A. Zarate Jr., H.K. Manji, Riluzole in psychiatry: a systematic review of the literature, *Expert Opin. Drug Metab. Toxicol.* 4 (2008) 1223–1234.
- [20] C. Pittenger, C. Vladimir, M. Banasr, M. Bloch, J.H. Krystal, G. Sanacora, Riluzole in the treatment of mood and anxiety disorders, *CNS Drugs* 22 (2008) 761–786.
- [21] M.C. Obinu, M. Reibaud, V. Blanchard, S. Moussaoui, A. Imperato, Neuroprotective effect of riluzole in a primate model of Parkinson's disease: behavioral and histological evidence, *Mov. Disord.* 17 (2002) 12–19.
- [22] D.L. Ginsberg, Riluzole for treatment-resistant obsessive-compulsive disorder, *Prim. Psychiatry* 12 (2005) 33–34.

- [23] T.J. Ritchie, P. Ertl, R. Lewis, The graphical representation of ADME-related molecule properties for medicinal chemists, *Drug Discov. Today* 16 (2011) 65–72.
- [24] T. Wąseka, J. Olczakb, T. Janecki, New, simple and versatile synthesis of protected α -alkylidene- β -amino acids from activated vinylphosphonates, *Synlett* 10 (2006) 1507–1510.
- [25] M. Fink, F. Duprat, F. Lesage, R. Reyes, G. Romey, C. Heurteaux, M. Lazdunski, Cloning, functional expression and brain localization of a novel unconventional outward rectifier K^+ channel, *EMBO J.* 15 (1996) 6854–6862.
- [26] H. Miranda, F. Sierralta, G. Pinardi, Neostigmine interactions with non-steroidal anti-inflammatory drugs, *Br. J. Pharmacol.* 135 (2002) 219–222.
- [27] E. Siegmund, R. Cadmus, G. Lu, A method for evaluating both non-narcotic and narcotic analgesics, *Proc. Soc. Exp. Biol. Med.* 95 (1957) 729–731.
- [28] S.L. Dixon, A.M. Smondyrev, S.N. Rao, PHASE: a novel approach to pharmacophore modeling and 3D database searching, *Chem. Biol. Drug Des.* 67 (2006) 370–372.
- [29] S.L. Dixon, A.M. Smondyrev, E.H. Knoll, S.N. Rao, D.E. Shaw, R.A. Friesner, PHASE: a new engine for pharmacophore perception, 3D QSAR model development, and 3D database screening: 1. Methodology and preliminary results, *J. Comput. Aided Mol. Des.* 20 (2006) 647–671.
- [30] T. Nagaoka, A.H. Bansjota, I.S. Tezuka, S. Kadota, Selective antiproliferative activity of caffeic acid phenethyl ester analogues on highly liver-metastatic murine colon 26-L5 carcinoma cell line, *Bioorg. Med. Chem.* 10 (2002) 3351–3359.
- [31] S. Saito, S. Kurakane, M. Seki, E. Takai, T. Kasai, J. Kawabata, Radical scavenging activity of dicaffeoyloxycyclohexanes: contribution of an intramolecular interaction of two caffeoyl residues, *Bioorg. Med. Chem.* 13 (2005) 4191–4199.